Journal of Alloys and Compounds 520 (2012) 22–29

Contents lists available at SciVerse ScienceDirect

Journal of Alloys and Compounds

journal homepage: www.elsevier.com/locate/jallcom

Magnetic and transport properties of $CePt_3Ge$ Kondo lattice in crystalline and sub-micron state

Jana Poltierová Vejpravová[a,*], Jan Prokleška[b], Jirí Pospíšil[b], Hideaki Kitazawa[c], Antonio Pereira Gonçalves[d], Takemi Komatsubara[e], Clemens Ritter[f], Olivier Isnard[f], Vladimír Sechovský[b]

[a] Institute of Physics of the AS CR, v.v.i., Department of Functional Materials, Na Slovance 2, 182 21, Prague 8, Czech Republic
[b] Charles University Prague, Faculty of Mathematics and Physics, Ke Karlovu 5, 121 16, Prague 2, Czech Republic
[c] National Institute for Material Science, Quantum Beam Center, Neutron Scattering Group, 1-2-2 Sengen, Tsukuba-shi, Ibaraki 305-0047, Japan
[d] Department of Chemistry, Instituto Tecnológico e Nuclear, 2686-953 Sacavém, Portugal
[e] Institute of Material Research, Tohoku University, 2-1-1 Katahira, Aoba-ku, 980-8577 Sendai, Japan
[f] Institute Laue Langevin, 6 rue Jules Horowitz, BP 156, F-38042 Grenoble Cedex 9, France

ARTICLE INFO

Article history:
Received 21 September 2011
Received in revised form
14 November 2011
Accepted 16 November 2011
Available online 9 December 2011

MSC:
1
2

Keywords:
$CePt_3Ge$
Kondo lattice
Short-range magnetic order
Size effect

ABSTRACT

We have studied a ternary phase of the $CePt_{3\pm x}Ge$ composition, with the maximum values of $x = 0.2$. A series of samples was prepared by arc melting, Czochralski method and splat cooling, and characterized by scanning electron microscopy and X-ray diffraction. The arc-melted samples are well-crystalline and single-phase with slightly varying stoichiometry close to the nominal $CePt_3Ge$, while the splat-cooled samples form an amorphous or a nanocrystalline constitution of the $\sim CePt_3Ge$ composition. Detailed measurements of magnetization, specific heat and electrical resistivity were performed in the temperature range 0.40–300 K, and magnetic fields up to 9 T. In addition, a delicate neutron diffraction experiment down to 70 mK was done, which excluded long-range magnetic order in the $CePt_3Ge$ compound. The specific heat data were tested to anisotropic Kondo model, and the resistivity behavior has been treated by means of electron localization effects. The experiments evidenced that the $CePt_3Ge$ compound can be considered as a Kondo lattice with low-temperature magnetic correlations, and the size effect seems to have minor role in control of the Kondo scattering phenomena in this compound.

1. Introduction

Cerium based intermetallic compounds are of considerable interest because of unusual physics arising from a single electron occupying the 4*f* shell of the Ce^{3+} ion. The single electron appears to be unstable against fluctuations of the spin and/or of the valence part into the conduction band, which lead to the presence of the typical low temperature anomalies on the electrical resistivity, magnetic susceptibility and specific heat [1]. Depending on the strength of mixing between the localized 4*f* and the conduction electron densities, variety of ground states can be recognized, ranging from fully localized Ce^{3+} to non-magnetic Ce^{4+}. The most exciting phenomena occur within the weak mixing regime, resulting in the Kondo-type or Kondo lattice behavior [2–5]. Those systems may exhibit heavy fermion superconductivity (HFSC), even in coexistence with magnetic order [6–8].

One of the key members of the HFSC family is the $CePt_3Si$, which is known as the first reported HFSC without center of inversion in its unit cell [9]. Beside the fascinating physical properties, its phase stability and formation of the non-centrosymmetric structure is worth of investigation in the context of potential isostructural phases with other rare-earth on the Ce site, Pd and Ni on the Pt site, and B, Al and Ge on the Si site, respectively.

The $CePt_3Si$ phase is isostructural to the $CePt_3B$ [10], and can be considered as a distorted tetragonal derivative of the $CePt_3$ cubic structure ($AuCu_3$ type structure), stabilized by the Si or B atom. Surprisingly, the cubic $CePt_3$ does not exists, in spite of the fact, that the $AuCu_3$-type structure is quite common among the binary 1:3 intermetallics [11]; the related phases $CeNi_3$ and $CePd_3$ do form [12,13].

The structural study of the $CePt_3Si$ analogues with other rare-earths has shown that the compounds with the light rare earths (RE = La to Sm, Gd) are isostructural, however those with a heavy

* Corresponding author. Tel.: +420 266 052 325.
E-mail address: vejpravova@seznam.cz (J.P. Vejpravová).

0925-8388/$ – see front matter © 2011 Elsevier B.V. All rights reserved.
doi:10.1016/j.jallcom.2011.11.086

Table 1
Summary of the $CePt_3Ge$ samples obtained by different procedures. Annealing treatment: Y/N – yes/no; cooling regime: S/Q – slow/quenched.

Label	Annealing	Cooling	Label	Annealing	Cooling
	Arc melted			*Grown*	
AM1	N	–	G1	N	–
AM2	Y	S	G2	N	–
AM3	Y	Q		*Splat-cooled*	
AM4	N	–	SC1	N	–
AM5	N	–	SC2	N	–
			SC3	Y	S

rare earth element (RE = Tb to Lu as well as Y) belong to a set of new structure types [14,15]. Recently, new ternary compounds $RPt_{3-x}Si_{1-y}$, $x = 0.17–0.22$, $y = 0.11–0.16$ (R = Y, Tb, Dy, Ho, Er, Tm, Yb) have been reported [16,17]. All members of the series adopt the same crystal structures (space group P4/mbm), which can be considered as a packing of four types of building blocks which derive from the $CePt_3B$-type unit cell by various degrees of distortion and Pt, Si-defects.

Beside, the physical properties of the stable $CePt_3B$ compound, other $CePt_3X$, where X is a *p*-metal, have been rarely investigated [18–20]. The most interesting study covers investigation of low-level Ge substitution in $CePt_3Si$ [20]. The authors have shown that the Ge atoms randomly occupy the 1*a* sites of space group P4/mmm up to 20 mol% of Ge. The monotonic increase of both *a* and *c* parameters yields a growing unit cell volume upon the Ge substitution. The Ge substitution simply drives a volume expansion, thus magnetism is stabilized and HFSC finally vanishes.

Other interesting problem arises when taking into account a mean size of the system and how it influences the weak mixing regime, in other words how the grain size modifies interplay of magnetic order and the Kondo scattering phenomena. Up to date, only few, but exciting reports of such kind have been published [21,22]. Chen et al. have shown that in Ce–Al intermetallic compounds, a crossover from magnetic ordering to an enhanced Kondo behavior occurs, possibly as a consequence of particle size and surface effects. As the particle size is reduced to nanoscale, the specific heat anomaly associated with the magnetic ordering diminishes, however the associated entropy exhibits a large increase. The authors of [22] presented a study of nanosized $CePt_2$. They observed that the antiferromagnetic correlations diminish with size reduction. They also propose that the lattice disorder is probably the origin of the variations of Kondo interactions and magnetic order for the larger nanoparticles.

In our work, we have focused on preparation and investigation of physical properties of a phase derived by replacing Si by Ge starting from the initial $CePt_3Ge$ composition. We have prepared the phase under various conditions and investigated its magnetic and transport properties. We especially focused on influence of the aggregation state on Kondo scattering phenomena by comparative investigation of a bulk and sub-micron sized samples.

2. Experimental

2.1. Sample preparation and characterization

We have prepared and investigated a series of samples, as summarized in Table 1. The nominal purity of the elements used for the preparation was: Pt–5N, Si–6N, Ce–3N. For comparison, we also used a piece of cerium metal purified by the solid state electrotransport (SSE) method [23]. The polycrystalline samples (labelled as AMx) were several times arc-melted under Ar (6N) protective atmosphere. Several attempts to grow a single-crystal by Czochralski method in tri-arc furnace (DCMP) were performed, however, without success; the obtained textured ingots were also investigated (samples Gx). For the splat cooling [24], 100–200 mg pieces of the as-cast polycrystalline button were used. Some of the samples were wrapped in tantalum foil, sealed in a quartz tube under vacuum and annealed at 900 °C for 1 week. For purpose of the specific heat data analysis, we also prepared an analogues compound with La by arc melting.

The samples were characterized using X-ray diffraction (XRD). The polycrystalline samples and ingot were investigated as powders, while the splat-cooled samples as bulk pieces. We used Seifert diffractometer equipped with Cu anode (Kα) and secondary monochromator in the Bragg–Brentano geometry. The data were analysed using WinPlotr package including the DICVOL program.

The microprobe analysis and direct observation of the microstructure of the samples, respectively, was performed on field-emission scanning electron microscope MIRA-XL (Tescan). The polycrystalline samples were carefully polished using 1 μm diamond paste, while the splat-cooled samples were studied directly.

2.2. Magnetization, specific heat and electrical resistivity measurements

All macroscopic experiments were performed using PPMS 9 T system (Quantum Design). For magnetization measurements, the polycrystalline samples were powdered and fixed in a gelatine capsule by instant glue. The splat-cooled samples were measured 'as obtained' in several orientations of the sample plate with respect to the applied magnetic field (no dependence on orientation of the magnetic field with respect to the sample plane was observed). The specific heat data were recorded on carefully polished sample plates with typical mass of 5 mg employing the two-tau relaxation method. The electrical resistivity was studied using standard four-probe configuration. The specific heat and electrical resistivity were also measured using ^{3}He system enabling to reach the minimum temperature of 0.40 K.

2.3. Neutron scattering

The neutron diffraction experiment was performed on D20 beamline in Institue Laue Langevin, Grenoble. For the purpose of the experiment, a dilution refrigerator was installed, and the diffraction patterns were recorded from 5 K to 0.07 K. The data were normalized to monitor and the analysis was done using the Lamp software.

3. Results and discussion

3.1. Remarks on synthesis

The melting procedure of the polycrystalline samples was smooth, we have not observed any difference when melting the components with the commercial or SSE treated Ce metal. In contrast, the crystal growth was stable enough to pull an ingot in case of the SSE purified Ce only. However, no single-crystal of the compound was finally grown in the tri-arc furnace (more then 10 trials were performed), one polycrystalline ingot was chosen for investigation (G1). Finally, a sample (G2) was also grown in the tetra-arc furnace in IMR using the pre-reacted components containing the SSE-treated Ce metal.

3.2. SEM analysis

The composition of the all samples does not vary significantly with respect to their preparation (as summarized in Table 2), while the microstructure is significantly different in case of the splat-cooled samples, as demonstrated in Fig. 1. Namely the SC2 sample shows an unusual structure constitutes of granules with average diameter from 100 nm to 2 μm. The polycrystalline samples exhibit slight variation of composition in some parts of the bulk piece, a detail of such area for the AM3 sample is also shown in Fig. 1. The main phase composition (light area) is 20.5:58.2:24.2, while that of the dark are corresponds to 20.5:58.2:21.3. The annealing procedure did not improved the homogeneity of the samples, but originated precipitation of small amount of another Ce:Pt:Ge phase, as shown in detail for the AM2 sample. Beside the major

Table 2
Phase composition of the samples obtained by microprobe analysis. The AM2-D and AM2-L correspond to the minority dark and light phase, respectively, recognized in the SEM images in Fig. 1.

	Ce	Pt	*Ge*		Ce	Pt	Ge
AM1	19.1	56.7	24.2	G1	20.0	58.9	21.1
AM2	20.5	58.2	21.3	G2	20.3	57.8	21.9
AM3	18.9	55.3	25.8	SC1	19.8	58.8	21.4
AM4	21.8	59.6	18.6	SC2	19.7	58.1	22.2
AM5	20.4	58.0	21.6	SC3	18.8	59.2	22.0
AM2-D	21.0	42.5	36.5	AM2-L	20.4	63.6	16.0

phase, additional ternary phase close to the 1:2:2 stoichiometry was observed. Similar changes were observed in the AM3 and SC3 samples. Therefore the cooling rate does not seem to be the driving factor for precipitation of the foreign phase after annealing at high temperature.

The phase composition of the La-compound was also checked by microprobe analysis yielding the resulting La:Pt:Ge ratio: 19.4:58.2:22.4.

3.3. X-ray diffraction

The XRD patterns of selected samples are depicted in Fig. 2. Obviously, the diffraction patterns cannot be indexed by the tetragonal $CePt_3B$-type structure and could not be satisfactorily described using the XRD patterns of the known ternary Ce–Pt–Ge structures and/or their superposition. Subsequently, we tried to analyse the experimental data using the indexing software DICVOL in order to obtain symmetry of the unit cell and cell parameters, respectively. The analysis was performed for the samples with reasonably defined Bragg peaks only (AM1, AM3, G2) and up to the orthorhombic symmetry.

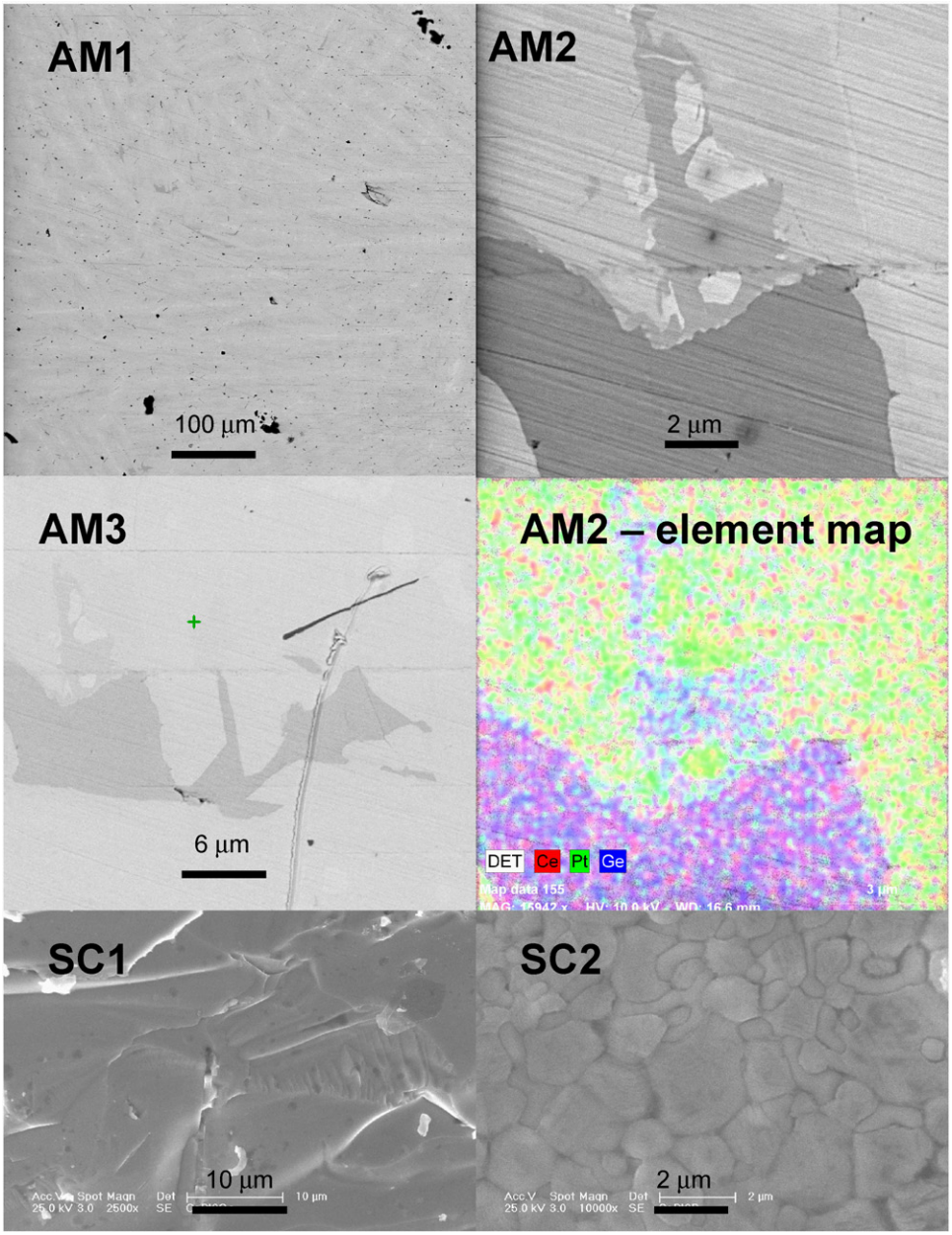

Fig. 1. Representative SEM images of the as-cast sample (AM1), annealed sample (AM2), and splat-cooled samples (SC1 and SC2), respectively. For the AM2 sample, the inhomogeneity regions with the corresponding Ce–Pt–Ge element-map is also shown.

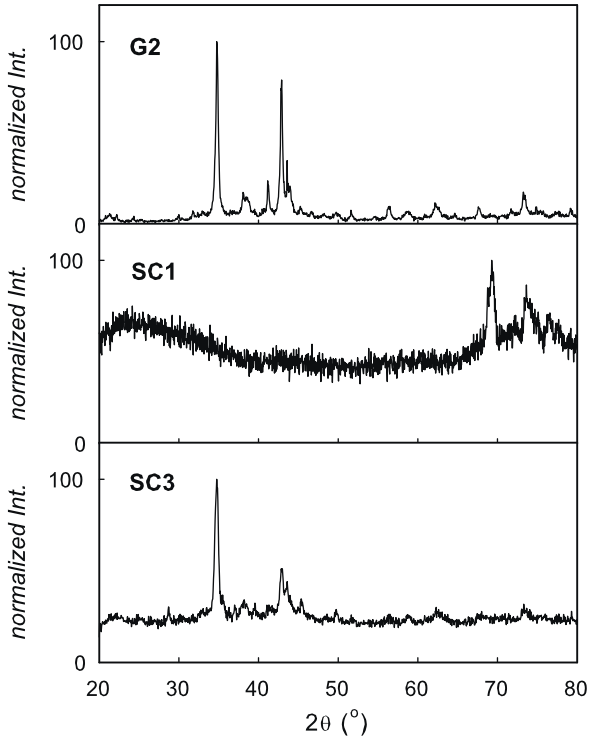

Fig. 2. Typical XRD patterns of a polycrystalline sample (G2, the 'ingot'), the as prepared (SC1) and the annealed (SC3) splat-cooled samples.

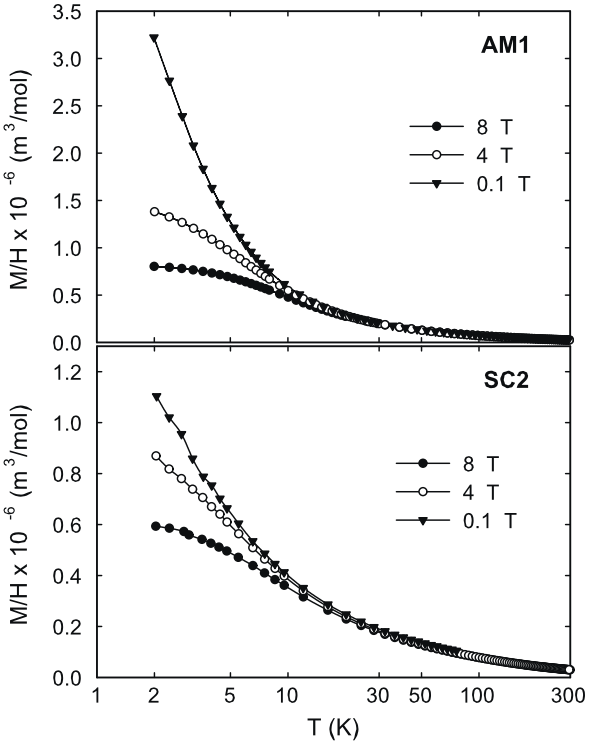

Fig. 3. Temperature dependence of the static magnetic susceptibility ($M/\mu_0 H$) at several magnetic fields.

Four possible structural arrangements reproduced the diffraction data. The space group and lattice parameters of the proposed structures are summarized in Table 3, the results do not correspond to any of those structures reported for RPt_3Si compounds with heavy rare earths. As they are composed of various types of building blocks derived from the $CePt_3B$-type unit cell, we have expected similar way of stabilization of the $CePt_3Ge$ structure leading to analogues or similar symmetry and dimensions of the unit cell. On the other hand, such analysis is only estimative and does not exclude the possibility of a related structure type.

The splat-cooled samples revealed either a broad bump in the diffraction data (Fig. 2, SC1) suggesting dominance of an amorphous fraction, or strongly enhanced intensities and diffraction peak widths (Fig. 2, SC3) induced by rapid cooling. Because the crystal structure is not unambiguously determined, further analysis of the data using a relevant texture and/or strain model was not performed. After annealing, the diffraction pattern resembles that of a polycrystalline sample (Fig. 3, SC3).

3.4. Magnetization and magnetic susceptibility

The results of the magnetic susceptibility and magnetization investigations of selected $CePt_3Ge$ samples are depicted in Figs. 3 and 4, respectively. There is no sign of magnetic ordering down to 2 K, and the temperature dependencies of the susceptibility do not significantly differ among the samples, as demonstrated in Fig. 3 for the AM1 and SC2 samples. Below 10 K, a field dependence of the susceptibility appears; while the low-field curve shows almost Curie–Weiss type behavior, the high-field susceptibility is significantly lower and tends to saturate on cooling. Similar trend can be observed in several heavy-fermion systems at low temperatures. An illustrative example is the CePtSi and CePtSi–Ge [26] with disorder-driven non-Fermi liquid (NFL)–Fermi liquid (FL) transition. The curvature of the temperature dependence of the susceptibility is interpreted as a result of two competing phenomena, the crystal-field splitting and spin disorder [26].

Table 3
Crystal structures proposed for the $CePt_3Ge$ compound, based on the data of the samples AM1, AM3 and G2.

	Space group	a (Å)	b (Å)	c (Å)
1	P4/mmm	7.743	–	26.358
2	Pmmm	13.440	8.034	2.592
3	P4/mmm	11.342	–	14.470
4	Pmmm	20.340	5.541	2.877

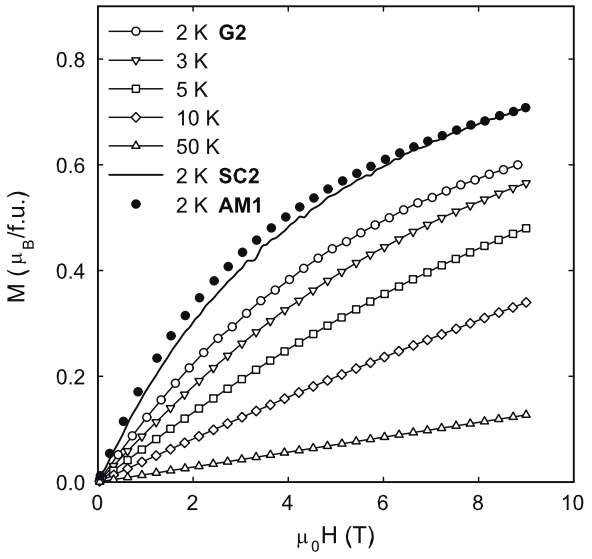

Fig. 4. Magnetization curves in the low-temperature region. All curves are shown for the G2 sample only. The black line and the black circles correspond to the SC2 and AM1 sample, respectively.

Table 4
Results of the susceptibility analysis, the error presented in the table represents the numerical error of the fit.

Sample	Modified CW			Standard CW	
	μ_{eff} (μ_B)	θ_P (K)	χ_0 (m^3/mol)	μ_{eff} (μ_B)	θ_P (K)
AM1	2.39 ± 0.05	−8 ± 1	3.3×10^{-8}	2.22 ± 0.05	−6 ± 1
G2	2.41 ± 0.04	−22 ± 2	2.1×10^{-8}	2.20 ± 0.05	−21 ± 3
SC1	2.49 ± 0.05	−26 ± 2	2×10^{-9}	2.49 ± 0.05	−26 ± 2

The susceptibility data were further analyzed by means of the modified Curie–Weiss (CW) law and the standard Curie–Weiss law ($\chi_0 = 0$) using the well-known formula:

$$\chi = \frac{C}{T - \theta_P} + \chi_0, \quad (1)$$

C is the Curie constant, θ_P is the paramagnetic Curie temperature, and χ_0 is the Pauli-type term. The results of the analysis are summarized in Table 4. The values are rather close to the Ce^{3+} free ion value. The data of the bulk samples are satisfactorily treated using the modified CW law, the obtained parameters are within those of other similar Ce-based compounds. The susceptibility of the SC2 sample, however, can be better described using the simple CW law suggesting suppression of the Pauli-type term contribution due to free electrons in the sample. This result could suggest suppression of the conduction electron density in the splat-cooled material, probably due to localization effects, as discussed further.

The magnetization curves of the grown sample G2 are presented in Fig. 4 together with the 2 K – curves of the arc-melted polycrystalline sample (AM1) and the splat-cooled sample (SC2). The more pronounced curvature of the M vs. $\mu_0 H$ curve in the arc-melted sample suggests presence of Ce^{3+}-impurities in the material as suggested also by the specific heat measurements (shown further). There are, however, no significant differences between the character of the magnetization curves among the sample series. The magnetization curves are Brillouin-type as expected for a paramagnetic system. They do not show any sign of metamagnetism up to 9 T in consistency with the monotonous in-field temperature dependence of the magnetic susceptibility. The value of the magnetic moment at 9 T/2 K is about 0.8 μ_B/f.u., which is within the range of other Ce-based Kondo compounds either without magnetic order or just above the ordering temperature.

3.5. Specific heat and magnetic entropy

The $CePt_3Ge$ was investigated in detail by the measurements of the specific heat down to 0.3 K and magnetic fields up to 9 T. We performed the measurements on the arc-melted (AM1, AM2, AM3), grown (G2) and splat-cooled samples (SC1, SC2), respectively. Comparison of the low-temperature specific heat data of the three representatives is shown in Fig. 5. Except an additional anomalies at around 1.8 K and 3 K due to small amount of an impurity phases in the annealed compound (AM2, not shown), the specific heat shows a distinct peak at $T \sim 0.6$ K in all investigated samples.

The temperature dependence of the C_p at various external magnetic fields is shown for the sample G2 (the most pure material). When applying magnetic field, the anomaly broadens and shifts to higher temperatures. Therefore we associate the anomaly with Kondo lattice condensation, however possibility of magnetic order cannot be excluded. The measure of redistributed entropy (isothermal entropy change, ΔS) and adiabatic temperature change (ΔT) due to the applied magnetic field, respectively, is shown in Fig. 6. The specific heat and caloric effects are not much affected by the splat-cooling procedure as demonstrated by the SC2 sample data.

To estimate the strength of the Kondo-type interaction in the system, the magnetic contribution to the specific heat C_{mag} and the magnetic entropy S_{mag} were calculated from the experimental data.

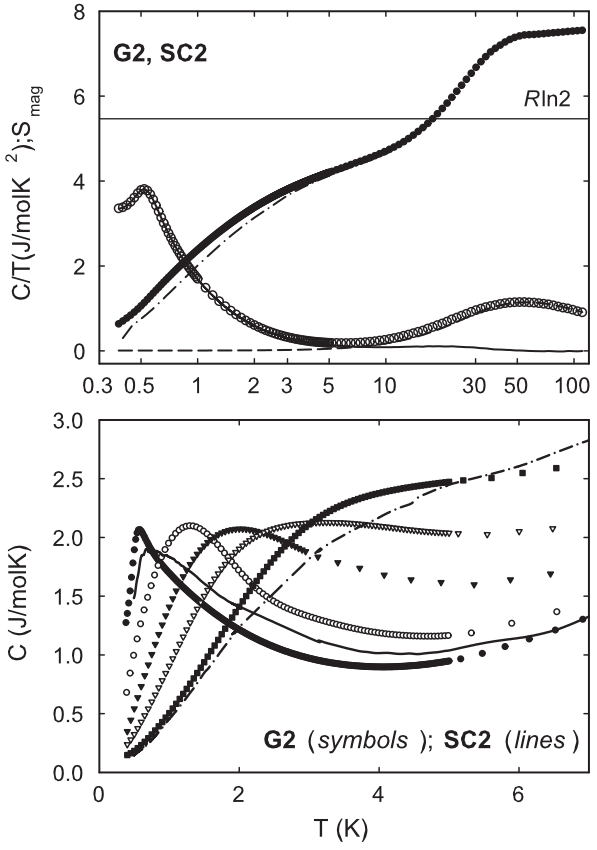

Fig. 5. Temperature dependence of the specific heat (C/T representation) – upper panel and its evolution in magnetic fields – lower panel. The fit of the electron and phonon contribution (C_{e+ph} solid line) and the extracted magnetic contribution (C_{mag}, dashed line) are shown in comparison to the zero field data. The magnetic entropy, S_{mag}, calculated from the C_{mag} is also presented (dash-dot line). The lower graph demonstrates continuous broadening of the specific heat anomaly in magnetic fields: 0 T, 1 T, 4 T, 6 T, and 9 T; the symbols correspond to the G2 sample, while the lines correspond to the zero field and in 9 T – field data of the S2 sample.

The specific heat analysis by means of combining the Debye and Einstein model is rather well-know, for details please see relevant references [25]. We assumed orthorhombic symmetry of the unit cell and consequently we applied a simplified grouping scheme for description of the optical phonon part within the Einstein model. The parameters describing the phonon and electronic contributions, obtained for the Ce-compound and its nonmagnetic analogue ($LaPt_3Ge$), respectively, are summarized in Table 5. The presented γ coefficient value is considered as the free electron contribution only. The specific heat enhancement due to electron correlations

Table 5
Parameters of the electronic and phonon specific heat. The n1 and n2 corresponds to the degeneracy number of the optical phonon modes.

	γ (J/mol K^2)	Θ_D (K)	Θ_{E1} (K)	n1	Θ_{E2} (K)	n2
$LaPt_3Ge$	7.0	108	150	8	280	4
$CePt_3Ge$	11.0	104	150	8	295	4

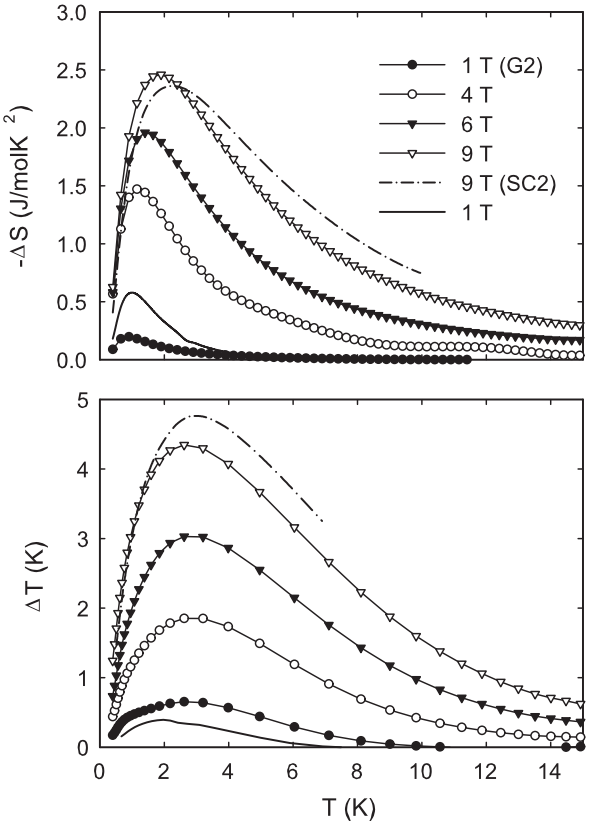

Fig. 6. Caloric effects in the G2 and SC2 samples.

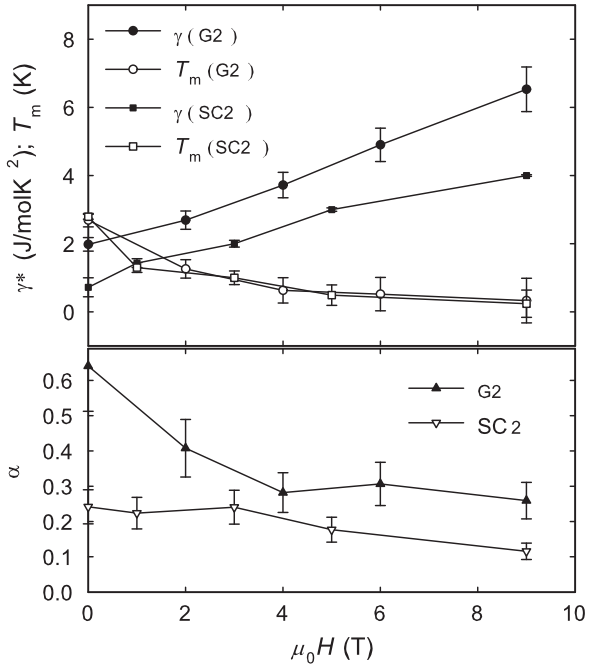

Fig. 7. Test of the anisotropic Kondo model.

and/or Kondo type interactions have been included in the 'magnetic' part, so the possible Schottky-type contribution. The obtained phonon spectra parameters do not differ significantly within the error of the analysis.

The low-temperature part of the magnetic entropy, S_{mag} is shown in Fig. 5 together with the magnetic part of the specific heat, C_{mag}. The S_{mag} reaches the doublet-related $R\ln 2$ value at around 25 K pointing to a considerable Kondo-type interaction in the system. The Ce^{3+}-related $R\ln 6$ value is reached at $\sim$ 140 K.

As we predicted at least tetragonal symmetry in the compound, an influence of anisotropy should be taken into account in interpretations of the specific heat data. The specific heat data were further submitted to the analysis in the frame of the anisotropic Kondo model [3]. The procedure was motivated by the study of the non-magnetic Kondo lattice compound $CeAl_2$ and its La-substituted derivative [4]. In a system with Ising-like crystal field ground state and strongly anisotropic exchange interaction in one crystallographic direction (e.g. the mentioned $CeAl_2$ case), the specific heat can collapse onto a universal scaling curve $C_p/\gamma T$ vs. T/T_m and the shift of the temperature of the peak on the C_p/T is given by $T_m = \alpha^* R/\gamma$, where α^* is a function of the uniaxial exchange parameter and the conduction-band density of states.

The shift of the T_m, γ-coefficient, and the calculated parameter α^* is shown in Fig. 7, respectively. The specific heat of the $CePt_3Ge$ reflects the main trends of the anisotropic Kondo model: the C_p-anomaly shifts to higher temperatures, the anomaly becomes broader and its maximum decreases, and the parameter α^* roughly decreases with increasing the magnetic field, as described in detail in Ref. [4].

In fact the specific heat data obtained by numerical treatment of the anisotropic Kondo model data can be strictly applied to a single-crystal with the magnetic field applied along the uniaxial direction, nevertheless, our results correspond to the main features of the proposed model much reliably then those presented in [4] for the La-substituted CeAl2.

3.6. Electrical resistivity and magnetoresistance

Fig. 8 presents typical temperature dependencies of resistivity for a melted, grown and splat-cooled sample, respectively. The relative decrease of resistivity on cooling is about 40% in the grown or polycrystalline material in contrast to the almost constant value in the splat-cooled samples. A specific resistivity at 300 K ranges from 78 μΩ cm in melted sample (AM1) to almost one order higher values 635 and 825 μΩ cm in the SC1 and SC2 splat-cooled samples. The value obtained for the grown sample (current applied parallel to the ingot axis) is 120 μΩ cm.

The MR curves of the grown sample are depicted in Fig. 9. Except a slightly varying absolute value of the MR, the trend of the MR dependencies is identical in all arc-melted and grown samples, respectively. In contrast, the splat-cooled samples show much different character of the MR curves and also much lower absolute MR values (approximately 10-times lower).

The detail of the low-temperature part of the electrical resistivity under applied magnetic field is shown in Fig. 10 for the SC2 sample. The resistivity shows a maximum at $T_{max}\sim$ 4 K and a logarithmic temperature dependence with a positive slope below T_{max} and with a negative slope above T_{max} up to ~20 K, respectively. The magnetic field causes a continuous decrease of the low-temperature resistivity and shift of the maximum to higher temperatures.

The reason for the observed character of the resistivity resides in the microstructure of the material. As it consists of ~100 nm grains, the resistivity much resembles that of granular metals in the border of the metal-insulator transition [27]. In those systems, the electrical resistivity is driven either by dominant electron localization or electron–electron interaction [28,29]. The dominance of the electron localization mechanism can be demonstrated by a linear dependence of the inverse resistivity on the square-root of the applied magnetic fields, which is usually fulfilled in high-enough magnetic fields in real systems [27]; above 3 T in case of our samples. The electron localization effect is corroborated by a linear

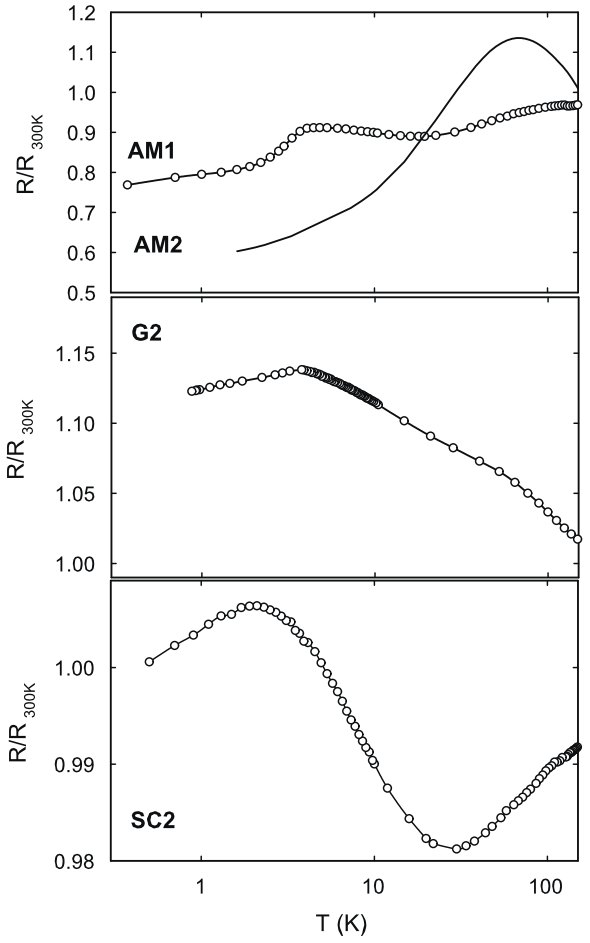

Fig. 8. Typical temperature dependencies of electrical resistivity of the AM1, G2 and SC2 samples.

behavior of the $1/R$ vs. $\sqrt{T}$ dependence, as depicted in Fig. 11. The linear section occurs only above the temperature of the resistivity maximum associated with the average Kondo temperature, which suggest dominance of Kondo lattice coherence at low-enough temperatures.

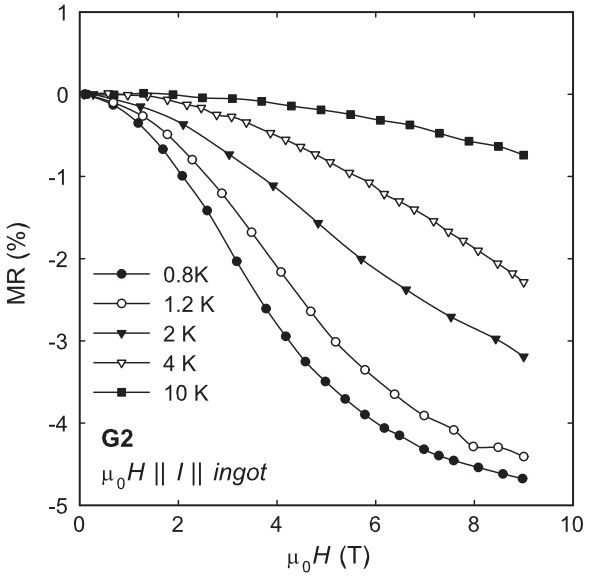

Fig. 9. Magnetoresistance (MR) of the grown sample, G2.

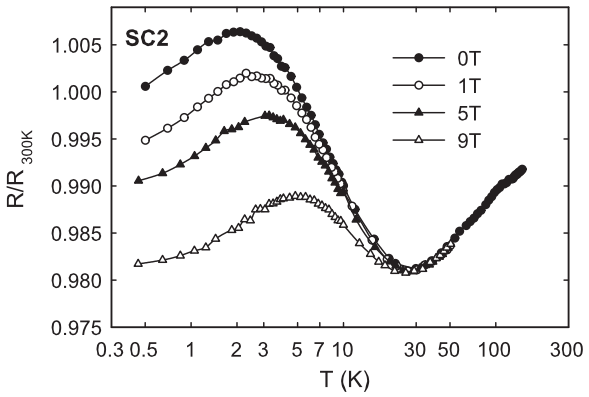

Fig. 10. In-field temperature dependence of the electrical resistivity of the splat-cooled sample SC2.

Finally, we will also discuss influence of disorder on MR in $CePt_3Ge$. As generally known, the Kondo temperature is very sensitive to a local disorder of ligands around the Ce ion, resulting in positive MR in low and negative MR in high magnetic fields, respectively. Beside the disordered 4*f* ligands, the so-called Kondo holes (a non-magnetic ion on a 4*f* ion site) play an important role, resulting in negative MR in all fields [5]. A test of the scenario can be done using a plot of magnetoresistance against magnetization. The plot based on the 2 K data is presented in Fig. 11 for the grown and splat-cooled samples. While the character of the SC2-curve does not fit to the Kondo disorder scenario, the MR vs. *M* dependence of the polycrystalline (grown) sample reveals surprisingly a dominant role of the Kondo holes as impurities in the MR of $CePt_3Ge$. The splat-cooled MR, however, is mainly driven by the electron localization phenomena discussed previously (Fig. 12).

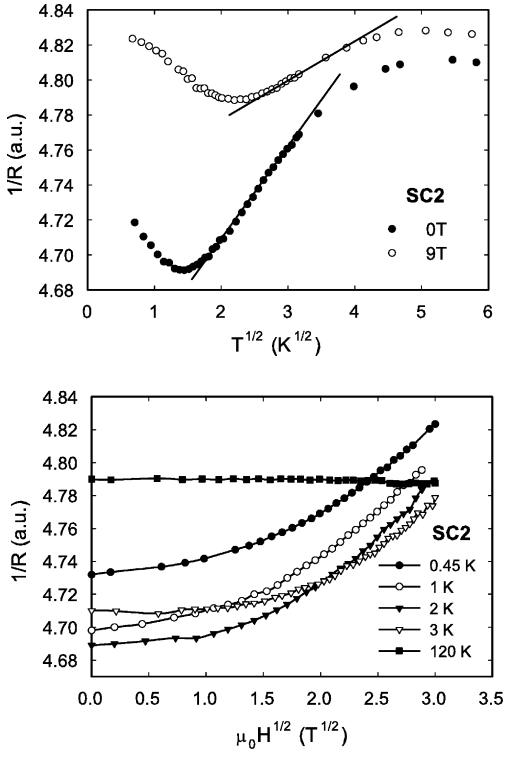

Fig. 11. Demonstration of the localization effects by means of the inverse electrical resistivity of the SC2 sample against the square-root of temperature (upper) and the square-root of the magnetic field (lower), respectively.

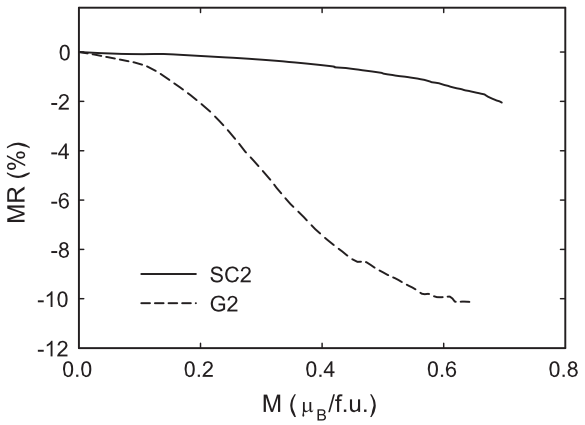

Fig. 12. Plot of the magnetoresistance (MR) vs. magnetization (*M*) demonstrating significant contribution of the Kondo holes to the MR.

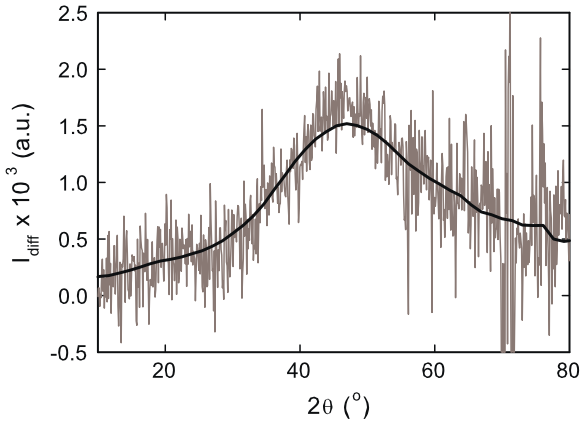

Fig. 13. Differential neutron diffraction intensity obtained by subtraction of the 5 K and 70 mK data.

3.7. Neutron diffraction experiment in the mK temperature region

The macroscopic investigations of the $CePt_3Ge$ compound did not unambiguously excluded magnetic ordering below 2 K. To inspect the possibility of long-range magnetic ordering or at least static magnetic correlations in the compound, a powder neutron diffraction experiment down to 70 mK was performed.

We observed no Bragg peaks due to magnetic scattering down to 70 mK indicating, that the long-range magnetic order lacks in $CePt_3Ge$. Fig. 13 demonstrates the differential magnetic intensity obtained by subtraction of the 5 K and 70 mK patterns. Because the crystal structure is not unambiguously determined, additional interpretation characteristic by means of correlation length was not performed. However, the data serve as a strong proof for presence of magnetic correlations in our Kondo lattice compound.

4. Conclusions

We have prepared a new phase with the composition close to the $CePt_3Ge$, and observed a significant difference in morphology of the melted and splat-cooled samples upon unchanged stoichiometry. Investigations of specific heat, magnetization and electrical resistivity, respectively, suggested, that the $CePt_3Ge$ is a Kondo lattice system. Results of neutron scattering experiments down to mK temperatures suggested, that magnetic correlations takes place on the background of the Kondo lattice phenomena, but long-range magnetic ordering does not develop. We also found out that the aggregation state has minor influence on specific heat and magnetization behavior, however, we discovered significant differences on electrical resistivity and magnetoresistance among the sample series. We have suggested the presence of localization effects in the splat-cooled samples. We conclude that the size effect is not essential for strong interruption of the Kondo lattice phenomena, as the characteristic coherence length is of two orders of magnitude lower than the mean grain size, and the weak-localization effect is originated mainly by lattice-spin disorder on the 100 nm to 1 μm scale, in consistency with the mean grain size of the splat-cooled sample.

Acknowledgements

The work was supported by the Grant Agency of the Czech Republic under project no. 202/08/P006. We acknowledge ILL for allocation of beam time for performing the neutron diffraction experiment and the ILL staff for support during the experiment. This work is a part of the research plan MSM 0021620834 and the project LG11024 both financed by the Ministry of Education of the Czech Republic.

References

[1] G.R. Stewart, Rev. Mod. Phys. 56 (1984) 755.
[2] J. Kondo, Prog. Theor. Phys. 32 (1964) 37.
[3] T.A. Costi, C. Kieffer, Phys. Rev. Lett. 76 (1996) 1683; T.A. Costi, C. Kieffer, Phys. Rev. Lett. 80 (1998) 1038.
[4] R. Pietri, K. Ingersent, B. Andraka, Phys. Rev. Lett. 86 (2001) 1090.
[5] F. Ohkawa, Phys. Rev. Lett. 64 (1990) 2300.
[6] H.V. Loehneysen, T. Pietrus, G. Portisch, et al., Phys. Rev. Lett. 72 (1994) 3262.
[7] Q. Si, F. Steglich, Science 329 (2010) 1161.
[8] W. Assmus, M. Herrmann, U. Rauchschwalbe, S. Riegel, W. Lieke, H. Spille, S. Horn, G. Weber, F. Steglich, G. Cordier, Phys. Rev. Lett. 52 (1984) 469.
[9] E. Bauer, G. Hilscher, H. Michor, et al., Phys. Rev. Lett. 92 (2004).
[10] S. Sullow, G.J. Niewuwenhuys, A.A. Menovsky, et al., Physica B 199 (1994) 644.
[11] E. Beaurepaire, G. Krill, J.P. Kappler, J. Rohler, Solid State Commun. 49 (1984) 65.
[12] D.T. Cromes, C.E. Olsen, Acta Crystallogr. 12 (1959) 689.
[13] J.M. Lawrence, J.D. Thompson, Y.Y. Chen, Phys. Rev. Lett. 54 (1985) 2537.
[14] A.I. Tursina, A.V. Gribanov, H. Noel, P. Rogl, Y.D. Seropegin, O.I. Bodak, J. Alloys Compd. 383 (2004) 239.
[15] O.L. Sologub, J.R. Hester, P.S. Salamakha, E. Leroy, C. Godart, J. Alloys Compd. 337 (2002) 10.
[16] A.I. Tursina, A.V. Gribanov, H. Noel, P. Rogl, Y.D. Seropegin, Acta Crystallogr. E 60 (2004) i8.
[17] A.I. Tursina, A.V. Gribanov, H. Noel, P. Rogl, Y.D. Seropegin, J. Alloys Compd. 395 (2005) 93.
[18] J. Vejpravova, J. Prokleska, V. Sechovsky, J. Alloy Compd. 408–412 (2006) 54.
[19] J. Vejpravova, J. Prokleska, V. Sechovsky, Physica B 359 (2006) 377.
[20] E. Bauer, G. Hilscher, H. Michor, et al., Physica B 359 (2005) 360.
[21] Y.Y. Chen, Y.D. Yao, C.R. Wang, W.H. Li, C.L. Chang, T.K. Lee, T.M. Hong, J.C. Ho, S.F. Pan, Phys. Rev. Lett. 84 (2000) 4990.
[22] Y.Y. Chen, P.H. Huang, M.N. Ou, C.R. Wang, Y.D. Yao, T.K. Lee, M.Y. Ho, J.M. Lawrence, C.H. Booth, Phys. Rev. Lett. 98 (2007) 157206.
[23] O.N. Carlson, F.A. Schmidt, D.T. Peterson, Proc. 10th Rare Earth Research Conf. CONF-730402-P2 II, 1973, p. 701.
[24] H. Jones, Rep. Prog. Phys. 36 (1973) 1425, and references there in.
[25] J. Vejpravova, J. Prokleska, B. Janousova, A.V. Andreev, V. Sechovsky, Physica B 797 (2006) 378.
[26] B.-L. Young, D.E. MacLaughin, M.S. Rose, et al., Phys. Rev. B 70 (2004) 024401.
[27] T. Chui, P. Lindenfeld, W.L. McLean, et al., Phys. Rev. Lett. 47 (1981) 1617.
[28] A. Kawabata, Solid State Commun. 34 (1980) 431.
[29] J.B. Bieri, A. Fert, G. Creuzet, et al., J. Phys. Met. Phys. 16 (1986) 2099.